ACS OMEGA

http://pubs.acs.org/journal/acsodf

Article

Exploring the Interactions of Ionic Liquids with Bio-Organic Amphiphiles Using Computational Approaches

Rachel E. Daso, Saige M. Mitchell, Charlotta G. Lebedenko, Ryan M. Heise, and Ipsita A. Banerjee*

Cite This: *ACS Omega* 2021, 6, 32460−32474

Read Online

ACCESS | Metrics & More | Article Recommendations | Supporting Information

ABSTRACT: Bio-organic amphiphiles have been shown to effectively impart unique physicochemical properties to ionic liquids resulting in the formation of versatile hybrid composites. In this work, we utilized computational methods to probe the formation and properties of hybrids prepared by mixing three newly designed bio-organic amphiphiles with 14 ionic liquids containing cholinium or glycine betaine cations and a variety of anions. The three amphiphiles were designed such that they contain unique biological moieties found in nature by conjugating (a) malic acid with the amino acid glutamine, (b) thiomalic acid with the antiviral, antibacterial pyrazole compound [3-(3,5-dimethyl-1*H*-pyrazol-1-yl)benzyl]amine, and (c) Fmoc-protected valine with diphenyl amine. Conductor-like screening model for real solvents (COSMO-RS) was used to obtain sigma profiles of the hybrid mixtures and to predict viscosities and mixing enthalpies of each composite. These results were used to determine optimal ionic liquid-bio-organic amphiphile mixtures. Molecular dynamics simulations of three optimal hybrids were then performed, and the interactions involved in the formation of the hybrids were analyzed. Our results indicated that cholinium-based ILs interacted most favorably with the amphiphiles through a variety of inter- and intramolecular interactions. This work serves to illustrate important factors that influence the interactions between bio-organic amphiphiles and bio-ILs and aids in the development of novel ionic liquid-based composites for a wide variety of potential biological applications.

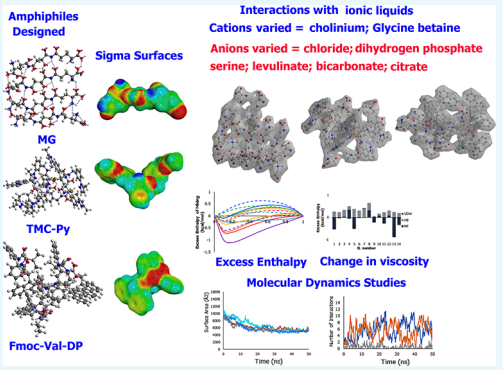

1. INTRODUCTION

Ionic liquids (ILs) are molten salts that are liquid below 100 °C and have unique thermal, physical, and electrochemical properties. Furthermore, their properties are highly tunable based on the specific cation−anion combination.[1] Over the years, ILs have been used as electrolytes and solvents for organic synthesis and battery applications, as well as to dissolve, extract, and purify proteins and other biomolecules.[2] ILs have also recently been explored for applications such as therapeutic materials, showing in some cases antimicrobial and drug delivery capabilities.[3] Of late, exploring the interactions of ILs with bio-organic molecules has become key to developing new ionic liquid composites for biotechnological applications.[4] However, due to the infinite combinations of cations and anions, the use of computational methods has become essential to predict the thermochemical properties and interactions of various ILs with bio-organic molecules. Computational approaches can aid in screening and optimizing IL cation/anion combinations for practical use to streamline their application in biological systems.

There are three main computational approaches that have been used and optimized for IL-bio-organic systems. Electronic structure methods, using *ab initio* or semiempirical calculations, for probing the system of interest in great detail, are typically used for smaller, static systems.[5] Density functional theory (DFT) is a semiempirical method that expresses the system in terms of the total electronic energy and allows for accurate and efficient measures of larger IL systems with multiple ion pairs. Specifically, for IL systems, correcting for dispersion with DFT-D theory accounts for the underestimation of van der Waals forces in typical DFT theory by introducing a Lennard-Jones-potential-like term. Such calculations have proven useful in probing noncovalent interactions between ILs and biomolecules.[6] Janesko used a DFT-D approach to model interactions between imidazolium chloride ILs with models of cellulose and lignin. The results indicated differing degrees of solubility based on the aromaticity and H-bonding capability of the ILs, as aromatic stacking and hydrogen-bonding interactions were found to be key to dissolution.[7] COSMO-RS, or conductor-like screening model for real solvents, is a priori of electronic structure methods that has been used to model ionic liquids.[8] The model calculates charge density over the surface of a molecule and is able to then predict thermodynamic properties about the molecule in

Received: July 21, 2021
Accepted: November 3, 2021
Published: November 19, 2021

a fluid system.[9] Liu and co-workers used COSMO-RS methods to screen the performance of over 600 IL combinations in the dissolution of keratin. Their study found that the main contributing factor in the IL dissolution of keratin was the number of H-bonding groups present in the IL.[10]

A second computational approach to probing IL-bio-organic systems involves the use of molecular mechanics simulations to visualize and analyze interactions between the ions and other components. These simulations involve both molecular dynamics (MD) and Monte Carlo (MC) methods. MD simulations explore the movement of a system over specific time points, while MC simulations sample random states weighed by the probability of moving to that state. Many MD approaches have been used to investigate IL systems. For example, Rabideau and co-workers used MD to analyze the interactions between cellulose and alkyl-imidazolium-based ILs. They found that during dissolution of the cellulose in the IL, a "patchwork" of cations and anions would form around the cellulose strand due to H-bonding and dispersion interactions and that increasing tail length on the cations showed a slight decrease in binding capability.[11] Another subset of molecular mechanics is molecular docking, a simulation that uses a sampling process and a scoring system to determine the best binding of a substrate to a binding pocket.[12] Singh and co-workers used docking to study the complexation process of lysozyme with a caffeine and dioctyl sulfosuccinate-based surface-active ionic liquid to study the interaction of the ions on the surface of the enzyme.[13] In a separate study, Saraswat and co-workers utilized docking approaches to screen pyrrolidinium, piperidinium, pyridinium, and imidazolium-based ILs for potential antiviral activity against SARS-CoV-2 protease.[14]

Another common approach involves coarse-grained methods that group molecules into "grains" that allow for quicker analysis of large-scale or long-term systems. Efforts have been made to expand the approach to IL ions so that they can be analyzed with systems with larger organic molecules. For example, Pérez-Sánchez and co-workers used a coarse grain approach to model the effect of choline-based ILs in the self-assembly of Pluronic copolymers. They were able to capture the morphological changes in assembly caused by altering the anions of the ILs, as well as how the addition of the IL to the aqueous assembly system altered the overall density of the formed micelle.[15]

While computational methods have been used to probe IL solvent systems for biomolecules, there has been less work considering the therapeutic use of ILs. Recently, the creation of bio-ILs (ILs that contain biologically derived cations or anions) has shown promise for the creation of novel ionic liquids with potential biological applications. For instance, Mukesh and co-workers developed pH-responsive nanogels from cross-linked choline polyacrylates that showed prolonged release of the chemotherapeutic drug 5-fluorouracil at low pH.[16] Annabi and co-workers conjugated bio-ILs composed of choline cations with gelatin methacrylol to create electrically conducting hydrogels that showed increased biocompatibility.[17] In another study, Kanaan and co-workers developed polycationic semi-interpenetrating *co*polymer networks by mixing chitosan and ionic liquid-based polymers and copolymers, such as poly(1-butyl-3-vinylimidazolium chloride) and poly(2-hydroxymethyl methacrylate-*co*-1-butyl-3-vinylimidazolium chloride). The IL hydrogels formed were shown to be mechanically stable and nonhemolytic and showed the increased release of lidocaine hydrochloride (LH) under electrical stimulation.[18]

While ILs containing imidazolium, pyrrolidinium, and pyridinium cations and a wide variety of anions have been studied in the formation of composites with polysaccharides and proteins,[19,20] to the best of our knowledge, there has been limited work on the development of composites of small molecule amphiphilic bio-organic compounds with bio-ILs. Recent studies have shown that some ILs can encourage the self-assembly of small amphiphilic molecules.[21] For example, Chen and co-workers reported that polarity and ionic charge of protic ionic liquids played a key role in the solubility of surfactants and stability of the amphiphile-IL systems. Certain protic ILs interacted with common small amphiphiles, such as hexadecyltrimethyl ammonium chloride, and form lyotropic liquid crystalline phases to micellular phases depending on the relative concentrations of the components.[22] Utilizing computational approaches to explore IL interactions with small amphiphilic biomolecules will prove to be crucial to defining the future role of ILs in the therapeutic realm.

In recent work, we have developed IL-peptide amphiphile-based hybrid systems. We have found that the incorporation of the amphiphilic molecules with ILs formed gelatinous materials with varying elastic properties.[23,24] The formation of these hybrids is driven by H-bonding and electrostatic interactions that play a large role in IL systems. In this work, using computational methods, we examined the ability of selected bio-ILs to form composite mixtures with the three newly designed bio-organic amphiphiles. Specifically, the interactions between 14 ILs and 3 newly designed amphiphiles were studied to predict potential mixing ability, thermal properties, and viscosities of the hybrids. The cations chosen were choline and glycine betaine, two common cations found in bio-ILs.[25,26] In general, choline and glycine betaine show more biocompatibility compared to imidazolium-based cations. While choline is a component of common phospholipids, betaine (trimethylglycine) is widely distributed in living organisms and physiologically plays an important role as an osmoprotectant and methyl group donor in biochemical pathways.[27] The anions studied include bicarbonate, citrate, dihydrogen phosphate, glucuronate, levulinate, serine, and chloride. These IL anions were selected to provide small monoanionic biomolecules with a range of electrostatic interaction abilities that are predicted to interact with the designed amphiphiles.[28]

The designed bio-organic amphiphiles include (i) N5-(4-((*R*)-4-amino-4-carboxybutanamido)-2-hydroxy-4-oxobutanoyl)-L-glutamine, in which the natural dicarboxylic α-hydroxy acid, malic acid (widely used in the food and cosmetic industry and also synthesized in vivo), was conjugated to the amino acid glutamine at both ends (MG) giving it amphiphilic properties. (ii) N^1,N^4-Bis(3-(3,5-dimethyl-1*H*-pyrazol-1-yl)benzyl)-2-mercaptosuccinamide in which the antibacterial compound [3-(3,5-dimethyl-1*H*-pyrazol-1-yl)benzyl]amine was conjugated to the two ends of thiomalic acid (TMC-PY). The compound thiomalic acid has been gaining interest, as it is commonly used in the preparation of various biologically active sulfur-containing drugs and has been found to induce apoptosis in HL-60 cancer cells.[29] (iii) (9*H*-Fluoren-9-yl)methyl (*R*) (1-(diphenylamino)-3-methyl-1-oxobutan-2-yl fluorenylmethyloxycarbonyl (Fmoc)-protected amino acid valine was conjugated with diphenyl amine (Fmoc-Val-DP). Fmoc-based peptides are known for their gelation ability and have been developed as

https://doi.org/10.1021/acsomega.1c03864
ACS Omega 2021, 6, 32460−32474

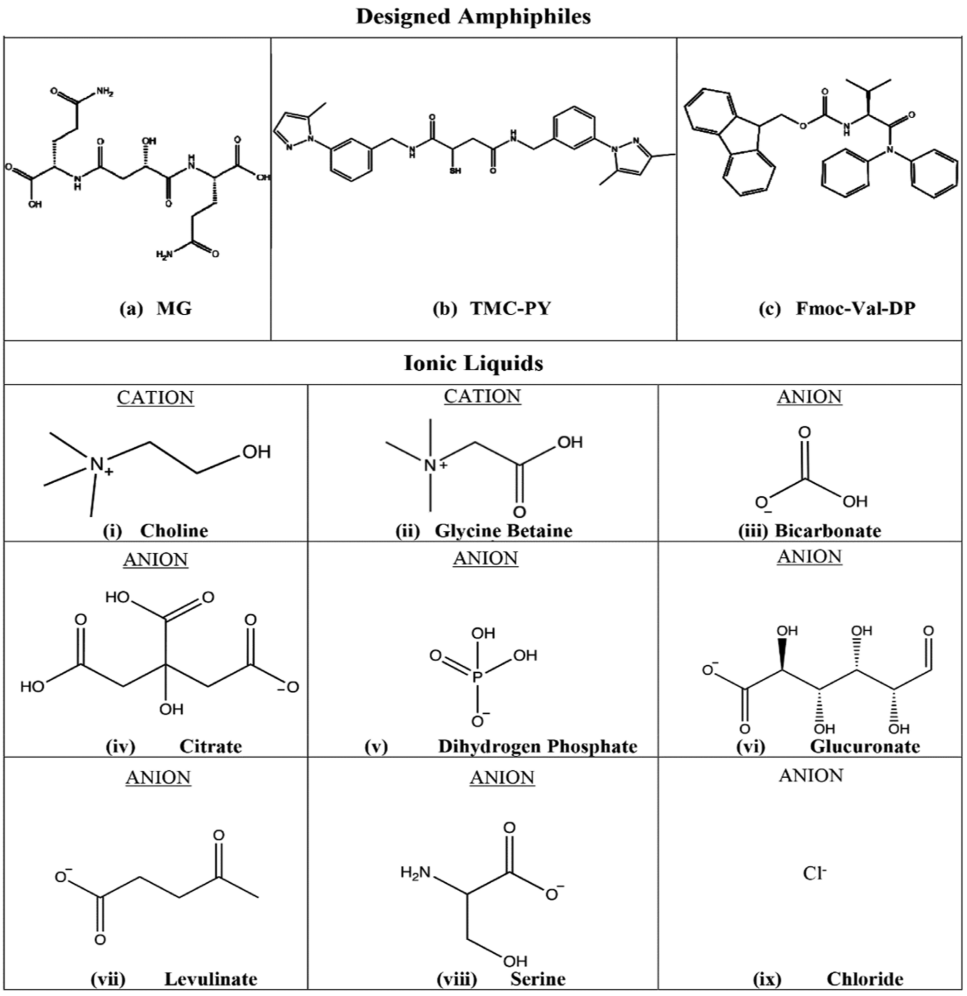

Figure 1. Top row: two-dimensional (2D) structures of the designed amphiphiles (a) MG, (b) TMC, and (c) Fmoc-Val-DP. Second row: (i) choline and (ii) glycine betaine are the IL cation components; and (iii) IL anion component bicarbonate. Third row: anion components of IL utilized (iv) citrate, (v) dihydrogen phosphate, and (vi) glucuronate. Fourth row: additional anion components of IL utilized (vii) levulinate, (viii) serine, and (ix) chloride.

potential carriers for drug delivery.[30] The structures of the designed bio-organic amphiphiles and the selected ILs are shown in Figure 1. These newly designed bio-organic amphiphiles provide a range of biological properties and hydrophobic and hydrophilic moieties. They are predicted to be capable of self-assembly due to a wide range of inter- and intramolecular interactions. Each of these compounds contains important biological moieties and was chosen to prepare hybrids with bio-ILs for potential biological applications.

We analyzed the effects of H-bonding, van der Waals interactions, and hydrophobic interactions involved in the formation of composites. We utilized COSMO-RS, COSMO-thermX, and molecular dynamics simulations to probe the interactions between the components and were able to classify and analyze the structural factors involved in the formation of bio-IL-amphiphile composites. The techniques shown in this work may be applied to screen IL-bio-organic hybrid mixtures and develop composites for possible biomaterial applications in the future. Furthermore, these studies can shed light on the physicochemical properties of novel IL hybrid bio-organic mixtures.

2. METHODOLOGY

2.1. Molecular Design. ChemDraw 18.0 was used to design the structures of the bio-organic molecules as well as the ILs (ChemDraw 18.0, PerkinElmer Informatics 2021). The three-dimensional (3D) structures were drawn on Chem 3D and energy-minimized using Chem 3D.

2.2. COSMO-RS Analyses. The electronic structure of the IL cations and anions and the bio-organic amphiphiles and their relative mixing energies were analyzed using COSMO-RS. The software COSMO-RS (conductor-like screening model for real solvents) uses a continuum solvation model to calculate the screening charge density on the surface of molecules and then uses this model to solve for chemical potential in solution, along with other thermodynamic data.[9,31] The COSMOS-RS calculations were carried out in a two-step process. The screening charge density sigma profiles for the ILs and amphiphiles were calculated with Turbomole.[32,33] An RI-DFT COSMO geometry optimization was performed utilizing the b−p functional and the def-TZVP basis set with standard settings. Excess enthalpy calculations of solid−liquid mixing of the amphiphiles in ILs were performed by COSMOthermX version 3.0 using parameter file BP_TZVP_C30_1301.[34] The COSMOtherm process for calculating excess enthalpy involves

https://doi.org/10.1021/acsomega.1c03864
ACS Omega 2021, 6, 32460−32474

three separate contributions depending on the electrostatic interactions occurring. The ΔG_{fusion} values for the amphiphiles were determined from DCS data. Further theory behind the method of calculation can be seen in the literature.[35]

2.3. Viscosity Analyses. Viscosity calculations were computed based on the multiple linear regression model proposed by Lemaoui and co-workers.[36] The model uses $S\sigma$ values, or areas of the sigma profile distribution, as a quantitative measure of the surface's polar screening charge. Several $S\sigma$ values were calculated, and certain regions were found to have a larger influence on viscosity values. The resulting expression depends on temperature. The relative viscosity values were calculated in terms of T to better understand the noncovalent interactions at play within the mixtures. $S\sigma$ values were calculated for each component in Mathematica[37]

$$\frac{\mathrm{Log}(\eta) + 0.02T}{(T - \bar{T})} = 0.62(S_5 - \overline{S_5}) - 0.60(S_6 - \overline{S_6}) - 2.69(S_7 - \overline{S_7}) - 3.09(S_9 - \overline{S_9}) - 18.64(S_{10} - \overline{S_{10}}) + 34.55(S_1 - \overline{S_1}) - 3.86(S_2 - \overline{S_2}) + 2.51(S_4 - \overline{S_4})$$

2.4. Molecular Dynamics. The molecular dynamics simulations were conducted using Desmond using the Schrodinger suite.[38,39] The geometry of the ILs and bio-organic amphiphiles was optimized with Gaussian using the PM3 semiempirical method.[40] The simulation box was prepared in Packmol, where 20 of the designed bio-organic amphiphiles and 20 IL molecules, 10 each of cation and anion, were packed into a 50 Å square box. The simulation box was prepared with the OPLS_2005 force field, which is an updated version of the all-atom optimized potentials for liquid simulation (OPLS-AA) force field. While there has been an additional parameterization of the OPLS-AA force field to better simulate the behavior of ILs, OPLS-AA force fields have been used to model IL mixtures and interactions as organic liquids with some success.[41] The box was solvated with SPC water molecules using the Desmond buffer method to create a box with a 10 A buffer between the edge of the box and the molecules of interest, and the box was packed to the appropriate density. Periodic boundary conditions were used in all directions.

To simulate the system, the Desmond workflow began with a Brownian dynamics NVT simulation (T = 10 K) with restraints on solute heavy atoms for 100 ps. Next, further NVT equilibration (T = 10 K) with restraints on solute heavy atoms was run for 12 ps followed by NPT equilibration (T = 10 K) with restraints on solute heavy atoms for 12 ps. Then, NPT equilibration (T = 300 K) with restraints on solute heavy atoms was run for 12 ps followed by NPT equilibration (T = 300 K) with no restraints for 24 ps. The Berendsen thermostat and barostat were used. The final MD production run was 50 ns with a time step of 1 fs and the NPT ensemble.

2.5. Run Analysis. Schrodinger's Maestro suite was used to calculate the root-mean-square deviation (RMSD), hydrogen bond count, solvent-accessible surface area (SASA), and radial distribution functions (RDFs) of the simulations. RMSD of the amphiphiles in the presence of ILs was calculated in reference to the 0th frame. Radial distribution functions were calculated by grouping molecules of interest by their center of mass. A maximum radius of 7.5 nm was used with a Δr of 0.01 nm. Trajectory files of the runs were also analyzed and imaged in the Maestro suite of Schrodinger.

3. RESULTS AND DISCUSSION

Understanding the interactions between ILs and biomolecules has proven key to developing IL novel materials for biological applications. In recent studies, it has been found that hydrogen-bonding interactions and hydrophobic interactions are key to IL−biomolecule interactions.[42] The IL cations chosen were choline and glycine betaine, two common cations used in bio-ILs. Choline and glycine betaine are also capable of hydrogen-bonding interactions through their hydroxyl and carboxyl groups, respectively. Many of the IL anions chosen are small molecules found in biological fluids (like bicarbonate, chloride, and phosphate) or amino acid derivatives (example, serine and levulinate) and thus are predicted to participate in hydrogen bonding in addition to electrostatic interactions with each other as well as with the designed amphiphiles.

The amphiphilic bio-organic molecules designed also differ in polarity, aromaticity, and hydrogen-bonding capabilities. MG contains several hydrogen-bonding acceptor and donor groups that can participate in electrostatic interactions. TMC-PY and Fmoc-Val-DP, however, have varying degrees of hydrophobicity and aromaticity due to the inclusion of conjugated ring systems. Additionally, MG, TMC-PY, and Fmoc-Val-DP contain functional groups, e.g., amides and carbonyl groups, that are also capable of H-bonding where TMC-PY contains slightly more hydrogen-bonding groups compared to Fmoc-Val-DP and MG most of all.

To study the interactions of the bio-organic amphiphiles, first sigma surfaces were generated by COSMO-RS. The geometries of all three amphiphiles were optimized, and the surface potential of the resulting geometries was determined. The resulting sigma profile is a histogram-like chart demonstrating the electrostatic potential of the sigma surface of the molecule. These three sigma profiles and corresponding sigma surfaces can be seen in Figure 2.

The sigma profiles indicate that the MG compound shows the least hydrophobicity and has more surface potential in the H-bonding donor and acceptor regions than the other two compounds. MG also has a very symmetric profile overall. The

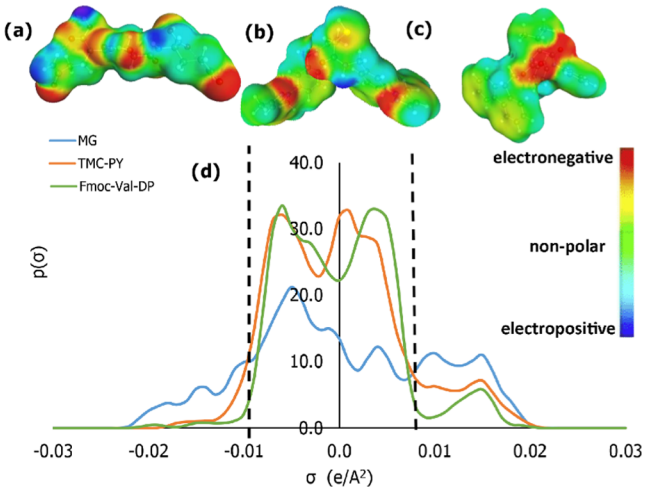

Figure 2. Three-dimensional (3D) sigma surfaces of (a) MG, (b) TMC-PY, and (c) Fmoc-Val-DP calculated by COSMO-RS methods; (d) corresponding sigma profiles of the three amphiphiles.

https://doi.org/10.1021/acsomega.1c03864
ACS Omega 2021, 6, 32460−32474

−0.015 e/Å^2 peak corresponds to the polar hydrogens in the hydroxyl group, and the +0.015 e/Å^2 peak corresponds to oxygen lone pairs. The peaks in the range of −0.01 and 0.01 e/Å^2 correspond to the slightly less polarized hydrogen on the −NH groups and the N lone pairs, respectively. The symmetric peaks at +0.005 and −0.005 e/Å^2 correspond to the carbon and hydrogen atoms in the carbon backbone, respectively. The symmetry of the profile indicates that the compound will act favorably with itself and thus has self-assembling potential.[43]

Both the Fmoc-Val-DP and TMC-PY have much greater density in the nonpolar range of the profile, which corresponds to the greater number of hydrophobic regions in both compounds. The symmetry of these regions with peaks around −0.005 and +0.005 e/Å^2 indicates that both will favorably self-assemble with primarily hydrophobic interactions. TMC-PY shows an additional peak around 0.01 e/Å^2 corresponding to the lone pairs on the nitrogen atoms in the pyrazole rings and the amide groups and one at +0.015 e/Å^2 corresponding to the oxygen atoms of the carbonyl groups. The profile, however, only shows a slight peak in the H-bond acceptor region because the polar hydrogen on the −SH group becomes trapped in the fold as the molecule folds in on itself to maximize the offset-stacked arrangement. The Fmoc-Val-DP profile shows a peak at +0.015 e/Å^2 corresponding to the lone pairs on the carbonyl oxygens in the carbon backbone. The fold of this molecule also limits the amount of exposure the nitrogen atoms have to the molecule surface, and thus, a second peak at 0.01 e/Å^2 is not observed. Overall, the general symmetry of both TMC-PY and FMOC-Val-DPA, especially in the nonpolar region, indicates their amphiphilic nature as well as their ability to self-assemble in aqueous solutions successfully.

The sigma profiles of the bio-organic amphiphiles were then compared to the profiles of the ILs. The ILs and their profiles are seen in Figure 3. The cations, glycine betaine, and choline have major peaks at −0.01 e/Å^2 representing the positively charged nitrogen atom. Glycine betaine has an additional peak at −0.02 e/Å^2, likely due to the hydrogen atom on the carboxyl group and a peak at +0.01 e/Å^2 due to the additional carbonyl group. As for the anions, all molecules have a peak around 0.02 e/Å^2 corresponding to the negatively charged oxygen or chlorine atoms. Phosphate shows two peaks in the H-bond donor region corresponding to the oxygen lone pairs and two peaks around −0.015 and −0.02 e/Å^2 corresponding to the hydroxyl hydrogens. Bicarbonate shows a very similar profile as phosphate, with the major anion peak being shifted to lower potential as phosphate is less electronegative than carbon. Citrate shows density across most of the lower potential levels with a notable peak around −0.02 e/Å^2 due to the hydroxyl oxygen. It shows a major peak at +0.013 e/Å^2 due to the carbonyl group oxygen atoms that are lower in potential than the region of the charged oxygen, which falls closer to the other anions at 0.02 e/Å^2. Levulinate shows uniquely two peaks in the hydrophobic region of the profile, which indicates that it may be complimentary to the amphiphiles and could participate in weak electrostatic interactions with those molecules. The serine anion also shows a peak in this range.

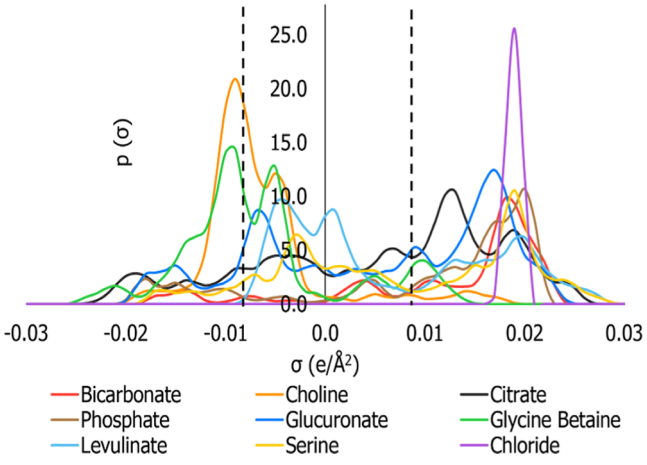

Figure 3. Sigma profiles showing the density of electrostatic potential over the surface of the molecule for IL cations and anions, as calculated by the COSMO-RS method.

Overall, to predict mixing with sigma profiles, complimentary of potentials is key. As MG is the only amphiphile with surface area in the −0.02 e/Å^2 range of potential, MG is most likely to mix favorably with the anions. As both cations show major peaks around −0.01 e/Å^2, both MG and TMC-PY have complimentary peaks at 0.01 e/Å^2 in their profiles, indicating that these amphiphiles will mix favorably with the cations. Levulinate, glycine betaine, and choline all have large peaks at −0.005 e/Å^2, which is also complimentary to the nonpolar regions of the amphiphiles, which indicates that these ions will mix favorably. Bavoh and co-workers found similar sigma profiles for glycine betaine and serine and found that broad peaks in the H-bonding regions, as well as shorter peaks in the nonpolar region of their profiles, would lead to favorable polarity for interactions in polar solvents.[44]

3.1. Viscosity Calculations. Sigma profiles can also be used to predict the viscosity of mixtures. The model proposed by Lemaoui et al. showed that while the sigma profile of ILs does not directly correlate to viscosity, certain regions of the profile do contribute to the change in viscosity with increasing or decreasing temperature. The sigma profiles were split into 10 regions, each 0.005 e/Å^2 in width ranging from −0.025 to 0.025 e/Å^2, where S1 corresponds to the region from −0.025 to −0.02 e/Å^2, S2 corresponds from −0.02 to −0.015 e/Å^2, and so on. Generally, they found that the regions that decreased viscosity with increasing temperature were regions S2, S6, S7, S9, and S10. S2, S9, and S10 are all the regions corresponding to medium- to high-polarity hydrogen-bonding donor and acceptor groups. Because these groups can form strong electrostatic interactions between molecules, the viscosity of a mixture is expected to decrease with increased temperature as these interactions are disrupted. Other regions, namely, S1, S4, and S5, result in a general increase in viscosity as temperature increases. This is due to the repulsive interactions of hydrophobic regions in the S4 and S5 regions as well as high-polarity HBA interactions. To analyze the IL interactions, we matched the two cations and seven anions into 14 different IL combinations seen in Table 1.

These IL numbers were used for the rest of the paper. The integral values S1−S10 were calculated for each IL combination, and they were used with the regression given by Lemaoui et al.[36] to calculate relative viscosity values with respect to temperature over the range of 278.15−368.15 K. The values are shown in Figure 4. The results indicate that all but two of the ILs were expected to decrease in viscosity with increasing temperature. This phenomenon is seen in many ILs

https://doi.org/10.1021/acsomega.1c03864
ACS Omega 2021, 6, 32460−32474

Table 1. Numbered IL Permeations and the Constituent Cations and Anions

IL number	cation	anion
1	choline	bicarbonate
2	glycine betaine	bicarbonate
3	choline	citrate
4	glycine betaine	citrate
5	choline	phosphate
6	glycine betaine	phosphate
7	choline	glucuronate
8	glycine betaine	glucuronate
9	choline	levulinate
10	glycine betaine	levulinate
11	choline	serine
12	glycine betaine	serine
13	choline	chloride
14	glycine betaine	chloride

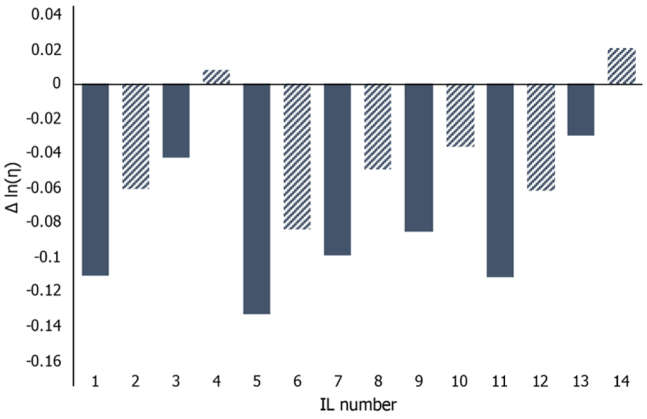

Figure 4. Predicted change in viscosity ($\ln(\eta)$) with an increase in temperature by 1 K for all 14 IL combinations. Solid bars are indicative of ILs with cholinium containing cations, while striped bars are indicative of glycine betaine ILs. Each of these contains different anions, as indicated in Table 1.

as favorable ionic interactions between the components result in decreasing viscosity with temperature.[45]

Ghatee and co-workers found that 1-alkyl-3-methylimidazolium ILs showed a similar decrease in viscosity with an increase in temperature due to the disruption of IL−IL noncovalent interactions. This often accounts for less viscous and more conductive materials at higher temperatures. In all cases, the ILs with the choline cation predict a greater decrease in viscosity per degree of temperature increase over the temperature range of 278.15−368.15 K. This is likely due to the highly charged carboxylic hydrogen peak in the sigma profile in the S1 region. The potential of this hydrogen atom is not able to be matched to a similar positive potential with the anion except with phosphate, which also has a significant sigma density in the 0.02−0.025 e/Å^2 region. This explains how IL6 with glycine betaine and phosphate is predicted to have the most negative relative viscosity of the ILs with glycine betaine. Of the ILs with choline, ILs1, 5, and 11 are predicted to have the greatest decrease in viscosity per temperature change. This is likely due to the broad and intense peaks of these three components at 0.02 e/Å^2. Because regions S9 and S10 correlated so strongly with a decrease in relative viscosity and stronger intermolecular interactions, these components with larger peaks in the 0.015−0.025 e/Å^2 regions were predicted to contribute to a greater decrease in viscosity. The value of IL viscosity depends on the synergistic effects of van der Waals forces as well as hydrogen bonding. It has been shown that quaternary amino acids show a significant decrease in viscosity with an increase in temperature due to this effect.[46] Other experimental studies have found that in choline-based ILs an increase in temperature disrupts the interactions between the anion and cation and generally causes a decrease in viscosity with an increase in temperature, which is in agreement with our results.[47]

The two ILs that were predicted to increase in viscosity with an increase in temperature were glycine betaine with citrate and chloride. Chloride anion is unusual as it does not have much electrostatic density outside of its Cl^- group to interact with glycine favorably. As glycine also has a highly electrostatic H group as well as density in the hydrophobic regions of the sigma profile, an increase in temperature would not necessarily disrupt particularly favorable interactions between the two. Citrate has a significant surface density in the −0.01−0.00 e/Å^2 range, which predicts an increase in viscosity as the temperature increases, as the hydrophobic areas of the molecule begin to be repulsed by the cationic glycine betaine. Generally, ILs are expected to decrease in viscosity with an increase in temperature. In the case of our study, citrate and chloride were two anions with unique sigma profiles that were not included in the anions studied by Lemaoui et al.,[36] and therefore, the slight increase in the viscosity with increased temperature is likely a result of the imperfect fit of the model to our specific data set. Because of this, the model overall is best suited to provide a relative ranking of viscosity and intermolecular forces of the IL combinations.

3.2. Thermodynamic Properties. The generation of sigma surfaces in COSMO-RS can also be used to calculate the thermodynamic properties of the molecules in mixtures. The excess enthalpy of mixing was then calculated in COSMOtherm for each IL with each of the three amphiphiles. The mixtures were calculated for a solid−liquid equilibrium (SLE) mixture where the IL is a liquid over the range of mole fractions of the amphiphile. The results obtained are shown in Figure 5.

Excess enthalpy is a thermodynamic property that can shed light on interactions that are formed or disrupted during the mixing of different components. The ideal mixing of a solid and liquid is not predicted to have a change in enthalpy, so the excess enthalpy of mixing indicates if the reaction will be endothermic or exothermic. The value of the excess enthalpy indicates the balance between the pure solvent and solute versus the mixed solution. A negative value indicates that the interactions in the mixture between two components are stronger than those between the pure components, and a positive value indicates the opposite.[48] COSMOtherm can split the calculated enthalpy values into contributions from misfit electrostatic interactions (H_MF), hydrogen-bonding interactions (H_HB), and van der Waals forces (H_VDW). All values are calculated by the potentials of the interacting surfaces, where hydrogen-bonding interactions are indicated by potentials above 0.08 e/Å^2 (noted by the dotted line in the sigma profile), misfit electrostatic interactions are below the threshold, and van der Waals interactions are only dependent on the number of atoms in the molecules. These split enthalpy values taken at a 50% molar composition indicate how the enthalpy is expected to change with respect to each of these interactions. It has been shown that while COSMO-RS has

https://doi.org/10.1021/acsomega.1c03864
ACS Omega 2021, 6, 32460−32474

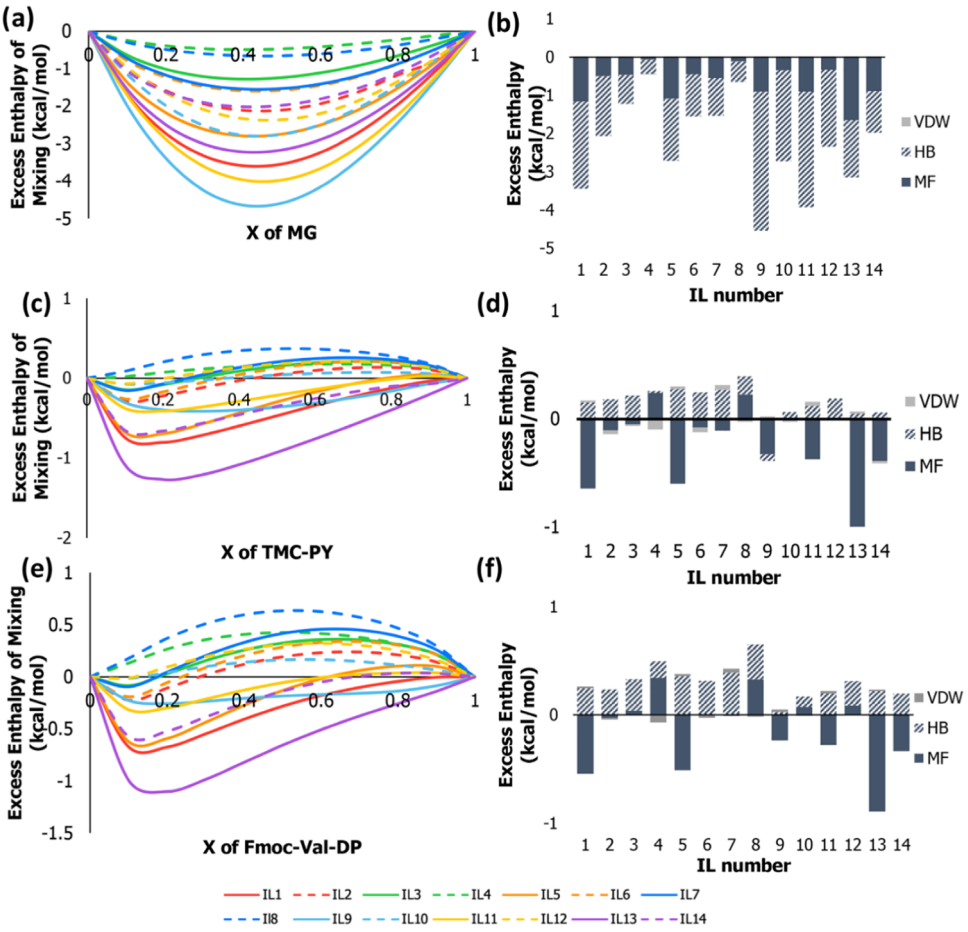

Figure 5. Estimated total excess enthalpy, H_m^E, of binary mixtures of ILs and amphiphiles: (a) MG, (c) TMC-PY, and (e) Fmoc-Val-DP at 298.15 K plotted against the mole fraction of the amphiphile. Predicted contribution of electrostatic misfit interactions ($H_{m,MF}^E$), hydrogen-bonding interactions ($H_{m,HB}^E$), and van der Waals forces ($H_{m,VDW}^E$) to the total excess enthalpy of the IL-amphiphile mixtures at a 50% mole ratio at 298.15 K for (b) MG, (d) TMC-PY, and (f) Fmoc-Val-DP. All IL combinations 1−14 are indicated in Table 1.

varying degrees of success with predicting quantitative excess enthalpy of mixing values, it is able to demonstrate trends and qualitative thermodynamic predictions with a fair amount of accuracy.[35]

For the MG amphiphile, excess enthalpies upon mixing with all 14 ILs were found to be exothermic with optimal mixing to be around 50% (Figure 5a). This indicates that the MG amphiphile will form favorable interactions with the IL cations and anions when dissolved. Among all IL combinations, choline ILs were seen to interact more favorably with the MG amphiphile than glycine betaine ILs with the same anion. This indicates that the hydroxyl group of choline can interact electrostatically more favorably with the side chain carboxyl groups as well as the amide groups of the amphiphile compared to the highly polarized carboxyl group on glycine betaine. The enthalpy contributions of MG also show that the different anions played a key role in creating a large range in excess enthalpy values. This indicates that the anions of the ILs are key for disrupting the hydrogen bonds present in the pure amphiphile material. This same key role of the anion was seen in the dissolution of keratin in several IL combinations.[10] We found that the anions levulinate, serine, and bicarbonate were able to disrupt the amphiphile interaction more strongly. These anions are capable of significant hydrogen-bonding and electrostatic interactions with the amphiphiles, indicating that such interactions are key to favorable IL−amphiphile interactions. The split enthalpy contributions also indicate that hydrogen bonds were predicted to be the dominant contribution to the favorability of MG mixing in ILs, followed by electrostatic interaction and with minimal contribution from van der Waals interactions (Figure 5b). This same pattern has been seen with interactions between other biomolecules at 298.1 K. For example, the binding of imidazolium ILs to double-helix DNA was found to have a negative excess enthalpy driven mainly by hydrogen-bonding and misfit interactions.[49] Keratin dissolution by a large range of imidazolium- and choline-based ILs also showed significant hydrogen-bonding interactions contributing to negative excess enthalpies of mixing.[10] Hydrogen bonds have also been predicted more broadly to be a unique force that facilitates IL−IL aggregates and plays a large role in the reactivity of IL systems.[50,51] As both MG and many of the ILs chosen are able to participate in hydrogen binding, their mixing is predicted to be favorable. The most favorable interactions were found between MG and ILs 9, 11, 1, and 13. These included ILs containing levulinate, serine, bicarbonate, and chloride. All of these components show favorable hydrogen-bonding interactions as well as electrostatic interactions, which were also indicated by complimentary areas of their sigma profiles.

The TMC-PY amphiphile also shows mixed interactions with the ILs, where six of the mixtures were predicted to be exothermic over majority of the mixture ratios (Figure 5c).

https://doi.org/10.1021/acsomega.1c03864
ACS Omega 2021, 6, 32460−32474

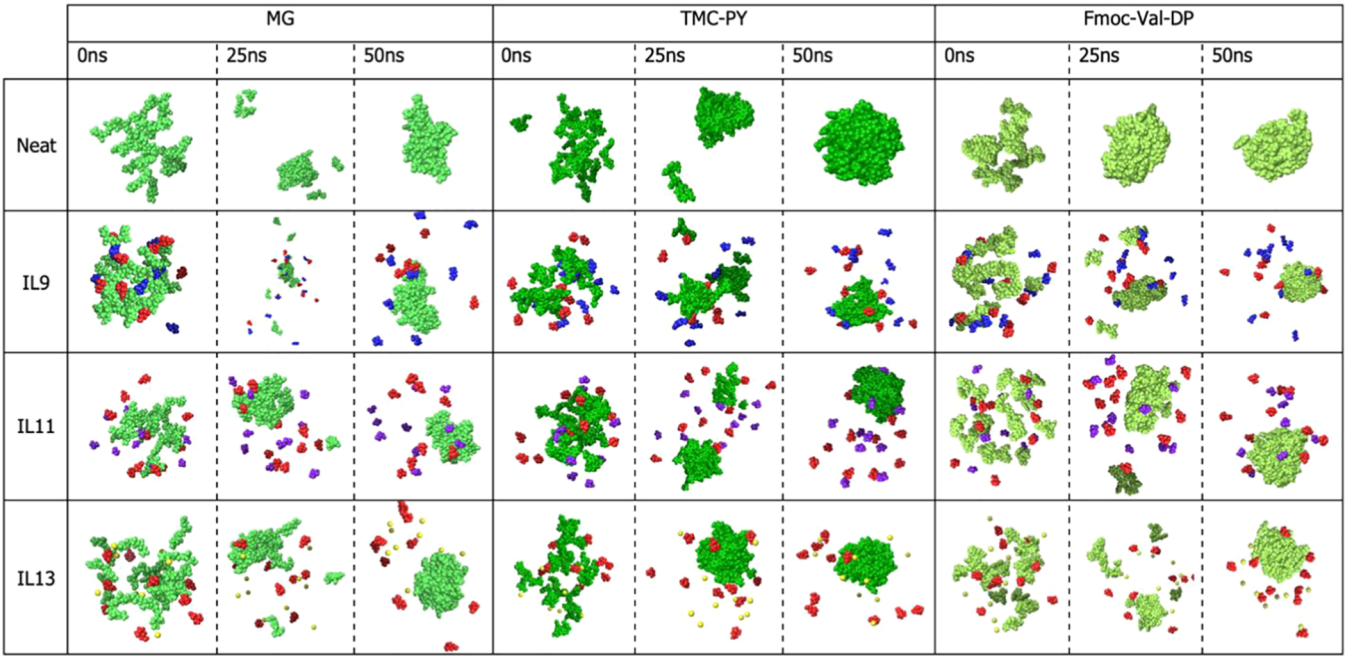

Figure 6. Comparison of trajectory snapshots of MD simulations of neat amphiphiles and composites of amphiphile-IL mixtures at 0, 25, and 50 ns. Green, amphiphile; red, choline; blue, levulinate; purple, serine; and yellow, chloride. Simulations were carried out in water, but water molecules were hidden for ease of viewing. Top row is indicative of neat assembly formation. Rows 2−4 are indicative of interactions of assemblies with cholinium levulinate (IL9), cholinium serine (IL11), and cholinium chloride (IL13), respectively.

The enthalpies of the mixtures were influenced most heavily by hydrogen-bonding and electrostatic misfit interactions, with minimal influence by van der Waals forces, which is expected as the molecules used were small. Overall, hydrogen bonding was less of an influence in these interactions and misfit electrostatic interactions began to play a larger role, especially in the overall exothermic mixtures (Figure 5d). This was likely because the TMC-PY amphiphile had a decreased hydrogen-bonding capability compared to the MG amphiphile. Hydrogen bonds are key in bio-organic molecule dissolution in ILs. Novoselov and co-workers found that cellulose dissolution was driven primarily by hydrogen-bonding interactions between the anions and the cellulose molecule,[52] and Scott and co-workers found that having strong hydrogen acceptors was key in anions for cellulose dissolution.[53] We see a similar effect here that the mixing becomes less energetically favorable as the TMC-PY amphiphile has a decreased hydrogen-bonding capability. In addition, we observed once again that ILs13, 11, 9, and 1 showed the most favorable interactions driven mainly by favorable misfit electrostatic interactions, while IL9 showed the only favorable hydrogen-bonding interactions.

Fmoc-Val-DP shows the least favorable mixing with the IL combinations, with only 6 of the 14 ILs showing exothermic mixing enthalpies at 50% composition (Figure 5e). In these cases, we again see the dominance of hydrogen-bonding and electrostatic interactions, where, in all cases, the hydrogen-bonding contribution to the mixing enthalpy is now positive (Figure 5f). Fmoc-Val-DP shows very little hydrogen-bonding capabilities, with its only real electrostatic potential in the H-bond range being in the 0.015 e/Å^2 area due to the carbamate group. There is less complimentary mixing to be predicted with this potential, and thus, Fmoc-Val-DP appears to prefer to hydrogen bond with itself as would the IL cations and anions. This explains why all IL combinations have about the same positive enthalpy contribution from hydrogen bonding, as it depends mainly on the cations that have similar potentials in the −0.015 e/Å^2 region. Electrostatic misfit interactions then become key to determining mixing capabilities. The most favorable interactions are predicted between ILs13, 1, and 9. The choline cation shows more favorable misfit interactions with Fmoc-Val-DP, which is why these are all choline ILs. Furthermore, the addition of bicarbonate, chloride, and levulinate also contribute to the misfit interactions to where the components are electrostatically compatible. Additionally, as there are fewer misfit interactions between Cl^- and choline, there is less disruption needed before combining with the amphiphile, which could account for its especially negative misfit enthalpy.

It is important to note that the sigma profiles and thermodynamic data above were calculated from a single lowest-energy conformation of the molecules, as calculated through the geometry optimization in the COSMO-RS minimization process. However, the molecules designed here are amphiphilic in nature and have rotatable bonds and thus have several conformations. Because sigma profiles involve surface charges, the surface of a molecule changes with a change in conformation and thus also will its sigma profile change. It has been shown that changing the conformation of the hydrogen-bonding region of a molecule can shift sigma profile peaks, where the shifts become more significant as the molecules become larger and more complex.[54] Using one conformation is generally acceptable for small molecules as considering several low-energy conformations of a molecule produces similar sigma profiles and thermodynamic COSMO calculations as considering only the lowest-energy conformation. However, with larger molecules with several hydrogen-bonding regions, the differences in profiles can be more drastic. It is worth noting that the nature of the following section of MD simulations is such that several different conformations of the amphiphiles occur throughout the simulation and that as

https://doi.org/10.1021/acsomega.1c03864
ACS Omega 2021, 6, 32460−32474

such may differ slightly from the expected results using a single lowest conformation.

3.3. Molecular Dynamics Simulations. To further probe the interactions of the ILs with the designed amphiphiles, we conducted molecular dynamics simulations using Desmond. We first conducted simulations to examine the assembly of the neat bio-organic amphiphiles using water as a solvent. The amphiphiles were placed in a 50 × 50 × 50 Å box using Packmol, and this was placed in the simulation box with a 10 A buffer to the edges of the box by Desmond. The entire 60 A × 60 A × 60 A ensemble was solvated with water, and the box was simulated for 50 ns. Figure 6 shows the trajectory images. The top row shows images of the neat amphiphiles throughout the simulations at 0, 25, and 50 ns.

As seen in the figure, in all runs, the amphiphiles were seen to pack into the center of the simulated box after 50 ns, indicating self-assembly at the amounts utilized for running the simulation. Such self-assembly is expected with larger amphiphilic molecules that can interact by hydrophobic and hydrophilic interactions. Self-assembly was not seen in simulations of the neat IL molecules (Supporting Information Figure S3). This indicates that the simulation could accurately depict the intermolecular interactions that are contributed by the amphiphiles in the presence and absence of ILs.

MG amphiphiles packed into amorphous assemblies forming globular structures over a period of 50 ns. At 25 ns, the amphiphiles are seen to bind significantly to each other but there are some individual amphiphiles that break off and rejoin throughout the simulation. The self-assembly of MG was driven primarily by hydrogen bonding between the −OH and −C═O---HN− as well as the free carboxyl groups. The neat TMC-PY amphiphiles packed into a more spherical assembly, which stayed packed firmly throughout the latter half of the simulation. This packing was primarily due to π-stacking interactions between pyrazole rings but there were also hydrogen-bonding interactions taking place between the nitrogen lone pairs and the exposed −C═O and −NH groups. We predict that there were also additional interactions between the exposed −SH groups, which lead to an efficient, spherical packing. The Fmoc-Val-DP amphiphiles packed very firmly into a spherical assembly that appeared very stable over the course of the simulation. This assembly was formed almost entirely due to quadrupolar interactions between the diphenylalanine groups, and packing was due to the hydrophobic effect.

We then chose to examine the effect of the ILs upon mixing with the amphiphiles by utilizing the three most thermodynamically favorable ILs from the thermodynamic study because those ILs were most likely to interact favorably with each of the amphiphiles. We ran 50 ns simulations after the addition of ILs 9 (cholinium levulinate), 11 (cholinium serine), and 13 (cholinium chloride). The corresponding trajectory images are seen in rows 2−4. As shown in columns 1−3, upon the addition of the ILs to MG, the MG amphiphiles again packed into an amorphous assembly, while the ILs remained separate in solution and did not pack significantly with the amphiphiles. There were some interactions observed with the choline cation and the levulinate and serine anions initially, but no significant incorporation within the amphiphile supramolecular structure was observed. At 50 ns, a minor incorporation of cholinium levulinate and cholinium serine ILs was observed with MG, but the cholinium chloride IL remained in the periphery. The interactions are likely due to exposed amide groups, hydroxyl groups, and free carboxyl groups on the MG amphiphiles that were able to interact favorably with the ILs. However, it is likely that the intramolecular interactions within the MG amphiphile were stronger and therefore the ILs did not incorporate as significantly.

For the TMC-PY amphiphiles in columns 4−6, with the addition of the ILs, the amphiphiles still reached a spherical assembly by the end of the simulation. We observed that upon the addition of IL9 (cholinium levulinate) and IL11 (cholinium serine), the cholinium, serine, and levulinate molecules were incorporated more favorably into the TMC-PY assembly and there are some morphological shifts in the self-assembled structure visible at 25 and 50 ns. However, upon the addition of IL13 (cholinium chloride), we observed fewer interactions between the IL anion and the amphiphiles. The polar groups of the serine, levulinate, and choline molecules were able to hydrogen-bond with the exposed carbonyl and −NH groups of the amphiphile, while cation−π interactions were likely the dominant force in self-assembly, which is why there was minimal disruption of the overall structure. In previous work, it has been shown that generally ILs encourage amphiphile and peptide self-assembly, where the introduction of more polar groups or longer alkyl chains of ILs can encourage further interactions.[55] The Fmoc-Val-DP amphiphiles with the ILs packed into similar spherical structures like the neat amphiphiles and appeared to interact very little with the ILs, indicating very little interactions with the ILs. This is likely due to the fact that the Fmoc-Val-DP molecules had the fewest number of hydrogen-bonding groups and the dominant quadrupolar interactions were not able to be disrupted by the weaker IL−amphiphile polar interactions.

The RMSD, or root-mean-squared deviation, of a run measures the structural difference between the initial frame and every subsequent frame and the overall stability of the assemblies. Results obtained are shown in Supporting Information Figure S1. As shown in the figure, the neat assemblies for MG, TMC-PY, and Fmoc-Val-DP show lower RMSD values compared to those obtained after incorporation of the ILs. This is indicative that the IL interacts with the assemblies causing changes in the assembly structure. In the case of neat MG, the RMSD values leveled off at 2.1 nm (with minor deviations (∼0.2 nm)) throughout the simulation, indicating that a stable assembly is formed by the end of the simulation. Upon incorporation of each of the ILs, the highest increase in RMSD was observed for IL13, (2.48 nm), indicating a change in the structure of the assembly due to interactions with the IL. In the case of ILs 9 and 11, the RMSDs initially showed deviations up to 20 ns and then stabilized at 2.4 nm, indicating that the assemblies were initially disrupted but later packed together into stable assemblies after 25 ns. For neat TMC-PY, the RMSD value decreases and remains stable between 10 and 40 ns and then decreases slightly and remains stable at 0.5 nm for the rest of the simulation. Upon incorporation of IL11 (cholinium serine), we observed an increase in RMSD to 1.4 nm, while in the case of IL9 and IL13, the RMSDs reached a value of 2.0 nm and 2.4 nm, respectively, indicating that the most stable composite was formed with the IL9 (cholinium serine). In the case of Fmoc-Val-DP, a very stable structure is formed as the simulation reached equilibrium within the first 10 ns and remained stable at 1.7 nm for the entirety of the simulation. Upon incorporation of the ILs, with Fmoc-Val-DP, the systems were found to equilibrate by 15 ns and the RMSD values were

https://doi.org/10.1021/acsomega.1c03864
ACS Omega 2021, 6, 32460−32474

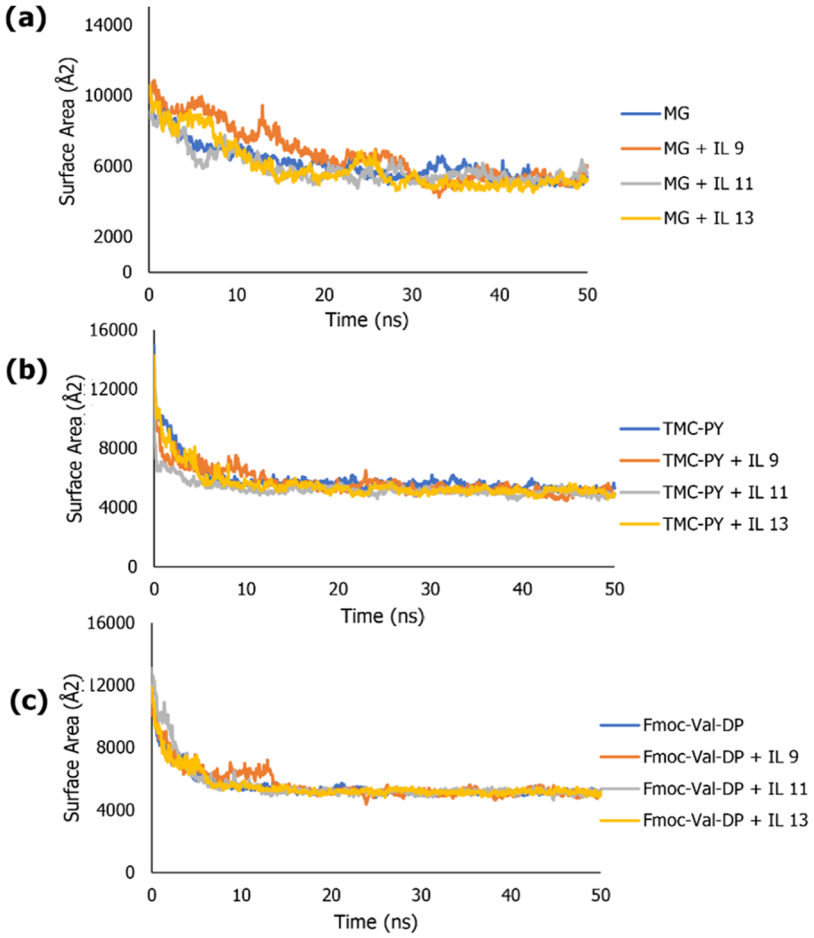

Figure 7. Total solvent-accessible surface area of the amphiphiles over 50 ns. Runs were conducted in a solvated box of 60 Å at STP. Charts show runs of (a) MG with and without the addition of ILs, (b) TMC-PY with and without the addition of ILs, and (c) Fmoc-Val-DP with and without the addition of ILs (IL9, cholinium levulinate; IL11, cholinium serine; IL13, cholinium chloride).

found to remain stable in the range of 2.6−2.8 nm for IL13 and IL11, while for the mixture with IL9, the system was found to stabilize at 2.5 nm.

To further elucidate these changes quantitatively, we examined the solvent-accessible surface area (SASA) of the bio-organic amphiphiles throughout the runs. Figure 7 shows the SASA of the amphiphiles in the presence of ILs 9 (cholinium levulinate), 11 (cholinium serine), and 13 (cholinium chloride). In all simulations, the accessible surface area decreases before leveling out. Such behavior is characteristic of self-assembly and was expected by the amphiphilic nature of the designed compounds.[56] In all cases, the MG amphiphile shows consistent final values of SASA but the process takes about 40 ns to reach equilibrium. This is likely due to the highly hydrophilic nature of the amphiphile, where water molecules can constantly interfere with packing, breaking amphiphiles off and allowing them to recombine. This back-and-forth process is seen in both the presence and absence of ILs, and it is demonstrated by the variability of the SASA values until reaching the end of the simulation. The SASA values averaged over the 10 final frames for the neat, IL9, IL11, and IL13 were 5359, 5814, 5818, and 5223 Å^2, respectively. The higher values of IL9 and IL11 suggest a greater disruption of packing, while IL13 seemed to encourage greater packing. This indicated that ILs with significant H-bonding capabilities can disrupt the assembly of polar amphiphiles, while ILs with fewer polar compounds could encourage further packing. The ILs did alter the self-assembly process as seen by inconsistencies in the SASA value and likely interrupted these interactions at several points in the simulation.

The SASA results for the relatively hydrophobic amphiphiles tell a different story. As can be seen for both TMC-PY and Fmoc-Val-DP, the SASA decreases rapidly and reaches a steady state after 15 ns. This state is highly conserved throughout the rest of the run, as seen by the lack of significant fluctuations in the data. This indicates tight packing that remains uninterrupted throughout majority of the simulation. This tight packing is likely due to the hydrophobic and aromatic nature of these amphiphiles, which, when placed in a polar solution, will aggregate tightly with little structural interruptions by the polar solvent. For Fmoc-Val-DP, the same spherical assembly is achieved with every solvent, both with ILs and without ILs, indicating that its propensity for self-assembly is driven naturally by hydrophobic interactions that are not then interrupted by other more polar solvents. The average final SASA values for neat, IL9, IL11, and IL13 were 5087, 4961, 5096, and 4969 Å^2, respectively. This supports that the packing was largely undisrupted by the addition of the ILs and if anything, polar interactions slightly increased the packing of the amphiphiles in the case of IL9 and IL13. The SASA graphs of TMC-PY also show neat packing, reaching a steady equilibrium around 15 ns in all simulations. There are larger fluctuations in the SASA values here compared to Fmoc-Val-DP, which is due to further disruption as TMC-PY has more

https://doi.org/10.1021/acsomega.1c03864
ACS Omega 2021, 6, 32460−32474

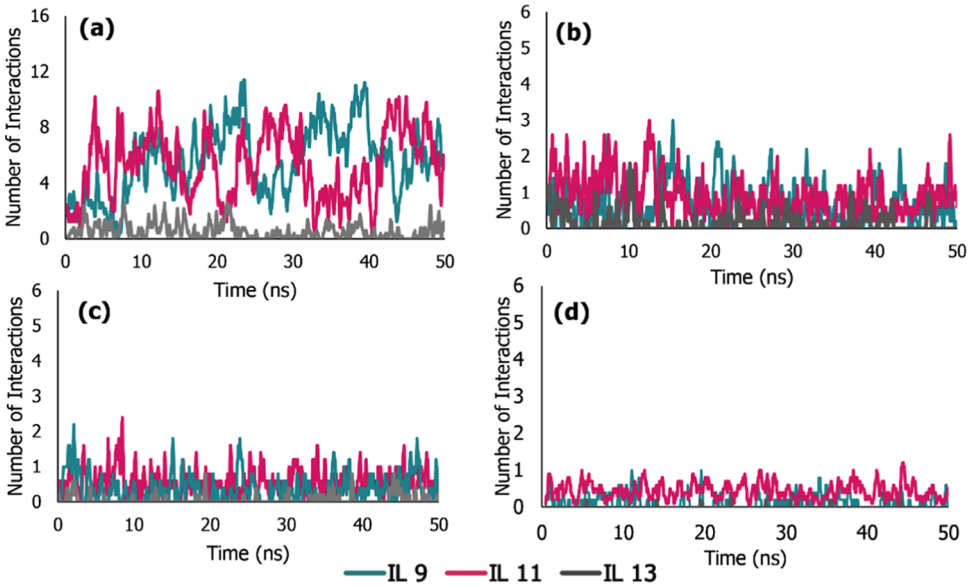

Figure 8. Comparison of the total number of hydrogen bonds between the ILs and ILs with amphiphiles over 50 ns. Runs were conducted in a solvated box of 60 Å at STP. Charts show runs of (a) MG with ILs, (b) TMC-PY with ILs, (c) Fmoc-Val-DP with ILs, and (d) neat ILs for comparison (IL9, cholinium levulinate; IL11, cholinium serine; IL13, cholinium chloride).

polar groups. The average final SASA values for neat, IL9, IL11, and IL13 were 5379, 4988, 4867, and 4852 $Å^2$, respectively. These values indicate a more significant effect from the addition of the ILs in further packing the TMC-PY assemblies. Especially with the addition of IL11 and IL13, the interactions between the ILs and the amphiphiles helped to encourage more efficient self-assembly.

To further explore the influences involved in the packing of these molecules, the number and types of intermolecular interactions were charted over the course of the simulations. The primary forces present in the assembly of the neat hydrophilic amphiphile MG were hydrogen bonds. The primary forces present in the packing of TMC-PY and Fmoc-Val-DP were pi stacking interactions as both of these compounds contained aromatic rings capable of these interactions. Figure S2 in the Supporting Information shows the number of these interactions between the amphiphiles throughout the neat assembly. For all three amphiphiles, the number of hydrogen bonds formed and pi−pi stacking interactions formed increase over the course of the assembly. These results support the fact that self-assembly driven primarily by hydrogen bonding and pi−pi ring stacking is taking place.

To specifically explore the impact that the ILs had on the amphiphile self-assembly, we examined the number of hydrogen bonds between these two components ignoring the amphiphile−amphiphile interactions. These results are seen in Figure 8. It is worth noting that these values are zero for the neat amphiphile and were very close to zero for the simulations run with the neat ILs (Figure 8d) averaging less than 0.5 hydrogen bonds per frame. The IL9 and IL11 had a significant number of hydrogen-bonding interactions with the amphiphiles, while IL13 showed fewer hydrogen-bonding interactions. The total number of hydrogen bonds was 5628 for IL9, 5380 for IL11, and IL13 had only 583 over the course of the simulation. This indicates that the anions of the ILs had more significant interactions with the amphiphiles than the cations, as IL13 had choline with chloride anions and shows much lower H-bonding counts throughout the simulations. This indicates that the ILs, and especially the anions, played a key role in the self-assembly of the MG amphiphiles through hydrogen-bonding interactions.

Because the TMC-PY amphiphile is more hydrophobic due to the presence of the pyrazole groups, there were fewer overall hydrogen bonds contributing to its self-assembly. With TMC-PY, over 50 ns, it can be seen again that IL9 and IL11 showed a greater number of hydrogen-bonding interactions compared to IL13. The total number of interactions were 736 for IL9, 914 for IL11, and 173 for IL13. This again demonstrates the importance of the anion in creating favorable interactions with the amphiphiles. It is likely that these hydrogen bonds contributed to further packing of the assemblies. Because TMC-PY has hydrogen-bonding capabilities due to the presence of the amide groups, it was able to interact with the ILs and its assembly was likewise influenced.

The Fmoc-Val-DP is predicted to have very little hydrogen-bonding capabilities. Likewise, the number of hydrogen bonds overall, as well as between the ILs and the molecules, was calculated to be very small for all three IL combinations. This indicates that the ILs had little influence in self-assembly of these highly hydrophobic amphiphiles due to their inability to interact through significant hydrogen bonding. Still, with the limited hydrogen bonding present, we see slightly more activity with ILs 9 and 11, choline-serine and choline-levulinate, respectively, which had 387 and 549 total interactions, respectively, than with IL13, choline-chloride, which only had 65. This same trend indicates that once again, the anion played a larger role in the ability of the IL to influence assembly, while overall hydrogen bonding plays a decreased role in impacting the assembly as the hydrogen-bonding capability of the amphiphile is decreased.

To further probe the self-assembly of the amphiphile-IL hybrid composites and examine the interactions between amphiphiles and ILs, radial distribution functions (RDFs) were calculated over the 50 ns MD trajectories. These results are seen in Figure 9. The RDFs for the simulations of neat

https://doi.org/10.1021/acsomega.1c03864
ACS Omega 2021, 6, 32460−32474

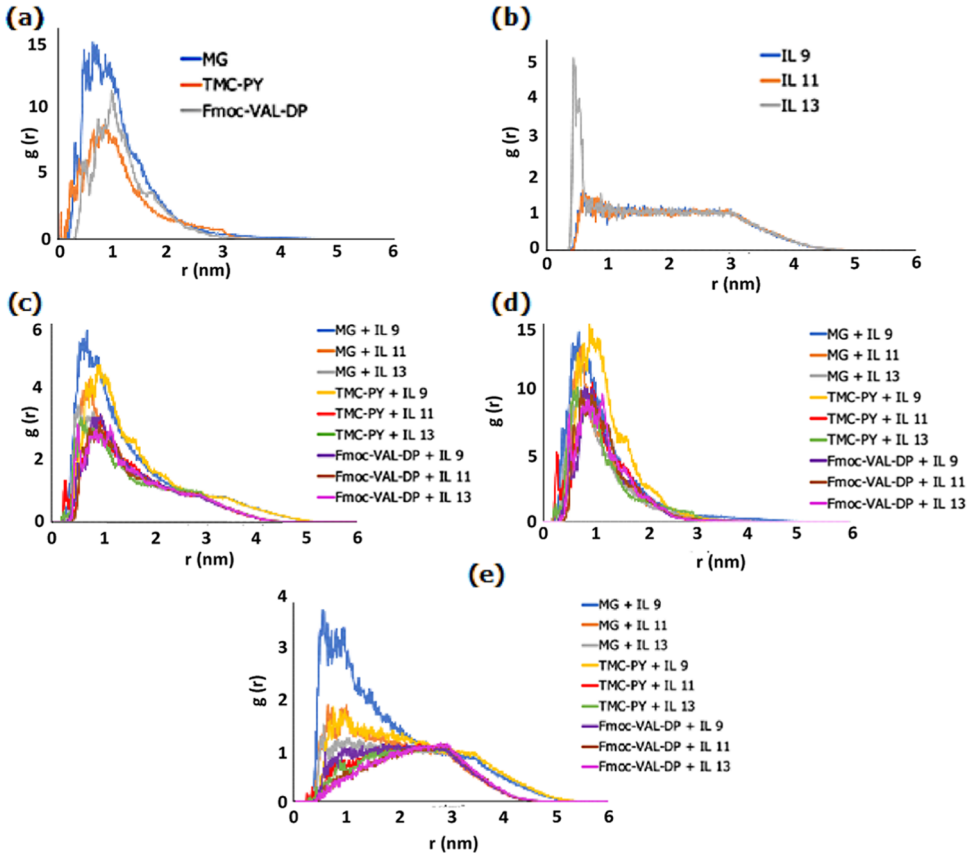

Figure 9. Radial distribution functions from MD simulations for (a) neat amphiphiles calculated between the center of mass of each amphiphile molecule, (b) neat ILs 9, 11, and 13 calculated between the center of mass of all IL components (cation and anion), (c) hybrids calculated between the center of mass of all molecules in the hybrid system (amphiphiles, cations, and anions), (d) hybrids calculated between the center of mass of each amphiphile molecule, and (e) hybrids calculated from the center of mass of cation and anion molecules to the center of mass of amphiphile molecules.

amphiphiles, calculated between all amphiphiles with each molecule represented by its center of mass, are shown in Figure 9a. On average, MG amphiphiles show the tightest packing upon self-assembly followed by TMC-PY and Fmoc-VAL-DP. For all three systems, all amphiphiles were found to be within about 3 nm of each other. No obvious peaks indicating structured assembly are seen in the RDFs. Fmoc-VAL-DP shows slight peaks around 0.4, 1.0, and 1.7 nm, suggesting that some distinct structures or layers might be present within the packing of the amphiphiles, but overall the distribution of the RDFs for the three amphiphiles suggests amorphous assemblies. Figure 9b shows the RDFs for the simulations of neat ILs 9, 11, and 13, calculated between both IL cation and anion with each molecule represented by its center of mass. The RDFs for ILs 9 and 11 suggest that no self-assembly occurs, with the RDF evenly distributed between 0.5 and 3 nm. The RDF for IL13 shows a sharp peak around 0.5 nm, suggesting that some self-assembly occurs among the salt, but the rest of the RDF closely mirrors those of ILs 9 and 11. These results indicate that little to no self-assembly occurs among the neat ILs in water. To further confirm this, trajectory image screenshots of the neat IL MD systems were used to show that no obvious self-assembly occurs throughout the 50 ns simulation (Figure S3).

Figure 9c shows the RDFs of the amphiphile-IL hybrids calculated between all components of the hybrid system (IL cation, IL anion, and amphiphile), with each molecule represented by its center of mass. The hybrid MG + IL9 showed the highest probability of all hybrid components being found near each other (within about 1 nm). Figure 9d shows the RDFs of the amphiphile-IL hybrids calculated between all amphiphiles in the system, with each molecule represented by its center of mass. These RDFs can be compared to the neat amphiphiles to assess how the addition of ILs to the system affected the packing of amphiphile molecules upon self-assembly. Overall, every hybrid system showed self-assembly of amphiphiles comparable to the self-assembly of neat amphiphiles, but differences were observed between the three ILs. For MG, IL9 allowed for the closest packing of amphiphiles, followed by IL11 and IL13. For TMC-PY, however, ILs11 and 13 allowed for closer packing of amphiphiles than IL9. The TMC-PY + IL9 hybrid appears to have the least tight packing of any amphiphile-IL hybrid. For the TMC-PY + IL11 hybrid, a sharp peak is seen around 0.25 nm followed by a large peak around 1.0 nm, suggesting that there was some structured layering within the amphiphile assembly. For Fmoc-VAL-DP, IL13 allowed for the closest packing of amphiphiles with sharp peaks also suggesting some structured layering, followed by IL11 and IL9. These RDFs demonstrate that each amphiphile might have a different IL that allows for ideal packing upon self-assembly. Overall, the RDFs show that all amphiphiles were found to be within approximately 3 nm of each other. Finally, Figure 9e shows the RDFs of the amphiphile-IL hybrids calculated from the IL

https://doi.org/10.1021/acsomega.1c03864
ACS Omega 2021, 6, 32460−32474

(both cation and anion components) to the amphiphile component, with each molecule represented by its center of mass. These RDFs show the probability of finding the IL components within a certain distance of the amphiphile assembly within the hybrid system. The MG + IL9 hybrid clearly shows the highest interactions between the IL and amphiphile components of the hybrid, followed by the MG + IL11 hybrid, MG + IL13 hybrid, TMC-PY + IL9 hybrid, and the Fmoc-VAL-DP + IL9 hybrid. This suggests that IL9 was most likely to actually incorporate into the assembly, whereas IL11 and IL13 were less likely to pack within the amphiphiles. Furthermore, IL9 was most likely to assemble with the MG amphiphile. Fmoc-VAL-DP was the least likely to incorporate ILs into its assembly, with IL11 and IL13 showing the least assembly. On average, the IL components were most likely to be located about 3 nm away from the Fmoc-VAL-DP components of those hybrids. It is important to note, however, that even for hybrids where the IL was not directly incorporated into the amphiphile assembly, the presence of IL in the system did have an effect on how the amphiphiles assembled in all cases.

These results further confirm that based on computational studies the amphiphiles designed here, particularly MG and TMC-PY, may have the potential to form layered composites with cholinium-based ILs and may be considered for laboratory synthesis and biological applications. The overall summary and key findings are shown in Figure S4.

4. CONCLUSIONS

In this work, we utilized COSMO-RS and MD simulations to probe the interactions between ILs and three newly designed bio-organic amphiphiles. Each of the amphiphiles possesses unique biological moieties with varying inter- and intramolecular interaction capabilities. We found that symmetric sigma profiles of the amphiphiles and the bio-ILs used here in (namely, [Chol][Ser] and [Chol][Lev]) proved to be key to influencing self-assembly. We also found that MG is predicted to mix favorably with the bio-ILs due predominantly to hydrogen-bonding capabilities of the amphiphile and ILs shown. TMC-PY was also predicted to mix in a thermodynamically favorable way with the ILs, with influence from both hydrogen-bonding, offset $\pi-\pi$ stacking, and electrostatic forces. Fmoc-Val-DP showed relatively less favorable mixing; however, in some cases, electrostatic interactions did prove to increase the favorability of mixing. The same influential role of hydrogen bonding was seen in self-assembly, where hydrogen bonding drove successful aggregation of the amphiphiles upon incorporation of the IL. We observed that for a hydrophobic amphiphile with hydrogen-bonding capabilities, the addition of the IL contributed to further packing compared to the neat amphiphile; however, with a more hydrophilic amphiphile, the addition of ILs can disrupt packing. Thus, it is possible that with tailored functional groups, IL-bio-organic amphiphiles may form due to favorable intermolecular interactions. These methods indicate that several computational techniques could be used in probing features of IL-bio-organic systems and shed light on the importance of the structures of the IL cations and anions and amphiphile functional groups for optimal IL−amphiphile interaction. Such systems may be considered for synthesis and development for a plethora of biological applications.

ASSOCIATED CONTENT

Supporting Information

The Supporting Information is available free of charge at https://pubs.acs.org/doi/10.1021/acsomega.1c03864.

RMSD analysis of the amphiphiles before and after incorporation of ILs (Figure S1); total number of $\pi-\pi$ interactions for TMC-DPA and Fmoc-Val-PY and total number of hydrogen bonds over 50 ns of MG (Figure S2); trajectory image screenshots of MD simulations for neat ILs 9, 11, and 13 (Figure S3); and summary of the design principles and key findings and design principles of this study (Figure S4) (PDF)

AUTHOR INFORMATION

Corresponding Author

Ipsita A. Banerjee − *Department of Chemistry, Fordham University, Bronx, New York 10458, United States;* orcid.org/0000-0002-6987-9717; Email: banerjee@fordham.edu

Authors

Rachel E. Daso − *Department of Chemistry, Fordham University, Bronx, New York 10458, United States*

Saige M. Mitchell − *Department of Chemistry, Fordham University, Bronx, New York 10458, United States*

Charlotta G. Lebedenko − *Department of Chemistry, Fordham University, Bronx, New York 10458, United States*

Ryan M. Heise − *Department of Chemistry, Fordham University, Bronx, New York 10458, United States*

Complete contact information is available at: https://pubs.acs.org/10.1021/acsomega.1c03864

Author Contributions

The manuscript was written through contributions of R.E.D., C.G.L., and I.A.B. I.A.B. was responsible for the conception of the project. R.E.D., C.G.L., S.M.M., and R.M.H. also worked on the acquisition of data. All authors have given approval to the final version of the manuscript.

Funding

The authors thank Fordham University for financial support of this work.

Notes

The authors declare no competing financial interest.

ACKNOWLEDGMENTS

R.E.D. thanks the Fordham University dean's office and the Clare Booth Luce Foundation for financial support of this work. R.E.D. and I.A.B. thank Upendar Thaduri for his technical assistance with the server and software-related matters. The authors also thank M. Whalen for helpful discussions.

ABBREVIATIONS

MG: N5-(4-((*R*)-4-amino-4-carboxybutanamido)-2-hydroxy-4-oxobutanoyl)-L-glutamine; TMC-PPY: N^1,N^4-bis(3-(3,5-dimethyl-1*H*-pyrazol-1-yl)benzyl)-2-mercaptosuccinamide; Fmoc-Val-DP: (9*H*-fluoren-9-yl)methyl(*R*)-(1-(diphenylamino)-3-methyl-1-oxobutan-2-yl)carbamate; IL: ionic liquid

https://doi.org/10.1021/acsomega.1c03864
ACS Omega 2021, 6, 32460−32474

REFERENCES

(1) Weingärtner, H. Understanding Ionic Liquids at the Molecular Level: Facts, Problems, and Controversies. *Angew. Chem., Int. Ed.* **2008**, *47*, 654−670.
(2) Benedetto, A.; Ballone, P. Room Temperature Ionic Liquids Meet Biomolecules: A Microscopic View of Structure and Dynamics. *ACS Sustainable Chem. Eng.* **2016**, *4*, 392−412.
(3) Egorova, K. S.; Gordeev, E. G.; Ananikov, V. P. Biological Activity of Ionic Liquids and Their Application in Pharmaceutics and Medicine. *Chem. Rev.* **2017**, *117*, 7132−7189.
(4) Tayyab, Z.; Safi, S. Z.; Rahim, A.; Khan, A. S.; Sharif, F.; Khan, Z. U. H. Preparation of cellulosic Ag-nanocomposites using an ionic liquid. *J. Biomater. Sci., Polym. Ed.* **2019**, *30*, 785−796.
(5) Keaveney, S. T.; Harper, J. B.; Croft, A. K. Computational Approaches to Understanding Reaction Outcomes of Organic Processes in Ionic Liquids. *RSC Adv.* **2015**, *5*, 35709−35729.
(6) Grimme, S. Density Functional Theory with London Dispersion Corrections. *Wiley Interdiscip. Rev.: Comput. Mol. Sci.* **2011**, *1*, 211−228.
(7) Janesko, B. G. Modeling Interactions between Lignocellulose and Ionic Liquids Using DFT-D. *Phys. Chem. Chem. Phys.* **2011**, *13*, 11393−11401.
(8) Han, J.; Dai, C.; Yu, G.; Lei, Z. Parameterization of COSMO-RS Model for Ionic Liquids. *Green Energy Environ.* **2018**, *3*, 247−265.
(9) Klamt, A. Conductor-like Screening Model for Real Solvents: A New Approach to the Quantitative Calculation of Solvation Phenomena. *J. Phys. Chem. A.* **1995**, *99*, 2224−2235.
(10) Liu, X.; Nie, Y.; Liu, Y.; Zhang, S.; Skov, A. L. Screening of Ionic Liquids for Keratin Dissolution by Means of COSMO-RS and Experimental Verification. *ACS Sustainable Chem. Eng.* **2018**, *6*, 17314−17322.
(11) Rabideau, B. D.; Agarwal, A.; Ismail, A. E. The Role of the Cation in the Solvation of Cellulose by Imidazolium-Based Ionic Liquids. *J. Phys. Chem. B* **2014**, *118*, 1621−1629.
(12) Salmaso, V.; Moro, S. Bridging Molecular Docking to Molecular Dynamics in Exploring Ligand-Protein Recognition Process: An Overview. *Front. Pharmacol.* **2018**, *9*, No. 923.
(13) Singh, G.; Kaur, M.; Kaur, H.; Kang, T. S. Synthesis and complexation of a new caffeine based surface active ionic liquid with lysozyme in aqueous medium: Physicochemical, computational and antimicrobial studies. *J. Mol. Liquids* **2021**, *325*, 115156.
(14) Saraswat, J.; Singh, P.; Patel, R. A Computational Approach for the Screening of Potential Antiviral Compounds against SARS-CoV-2 Protease: Ionic Liquid vs Herbal and Natural Compounds. *J. Mol. Liq.* **2021**, *326*, No. 115298.
(15) Pérez-Sánchez, G.; Schaeffer, N.; Lopes, A.; Pereira, J. F. B.; Coutinho, J. A. P. Using Coarse-Grained Molecular Dynamics to Understand the Effect of Ionic Liquids on the Aggregation of Pluronic Copolymer Solutions. *Phys. Chem. Chem. Phys.* **2021**, *23*, 5824−5833.
(16) Mukesh, C.; Bhatt, J.; Prasad, K. A Polymerizable Bioionic Liquid Based Nanogel: A New Nanocarrier for an Anticancer Drug. *Macromol. Chem. Phys.* **2014**, *215*, 1498−1504.
(17) Noshadi, I.; Walker, B.; Portillo Lara, R.; Shirzaei, E.; Gomes, N.; Aziziyan, M. R.; Annabi, N. Engineering Biodegradable and Biocompatible Bio-Ionic Liquid Conjugated Hydrogels with Tunable Conductivity and Mechanical Properties. *Sci. Rep.* **2017**, *7*, 4345.
(18) Kanaan, A. F.; Piedade, A. P.; de Sousa, H. C.; Dias, A. M. A. Semi-Interpenetrating Chitosan/Ionic Liquid Polymer Networks as Electro-Responsive Biomaterials for Potential Wound Dressings and Iontophoretic Applications. *Mater. Sci. Eng., C* **2021**, *121*, No. 111798.
(19) Takada, A.; Kadokawa, J. Fabrication and Characterization of Polysaccharide Ion Gels with Ionic Liquids and Their Further Conversion into Value-Added Sustainable Materials. *Biomolecules* **2015**, *5*, 244−262.
(20) Belviso, B. D.; Caliandro, R.; Salehi, S. M.; Di Profio, G.; Caliandro, R. Protein Crystallization in Ionic-Liquid Hydrogel Composite Membranes. *Crystals* **2019**, *9*, No. 253.
(21) Greaves, T. L.; Drummond, C. J. Ionic Liquids as Amphiphile Self-Assembly Media. *Chem. Soc. Rev.* **2008**, *37*, 1709−1726.
(22) Chen, Z.; Greaves, T.; Fong, C.; Caruso, R.; Drummond, C. Lyotropic Liquid Crystalline Phase Behaviour in Amphiphile−Protic Ionic Liquid Systems. *Phys. Chem. Chem. Phys.* **2012**, *14*, 3825−3836.
(23) Whalen, M.; Daso, R.; Thomas, M.; Banerjee, I. Interactions of Betainium and Imidazolium-Based Ionic Liquids with Peptide Amphiphiles and Their Implications in the Formation of Nanohybrid Composite Gels. *J. Sol-Gel Sci. Technol.* **2021**, *97*, 1−17.
(24) Daso, R.; Osborn, L.; Thomas, M.; Banerjee, I. Development of Nanoscale Hybrids from Ionic Liquid−Peptide Amphiphile Assemblies as New Functional Materials. *ACS Omega* **2020**, *5*, 14543−14554.
(25) Pereira, M. M.; Almeida, A.; Gomes, J.; Rufino, A. F.; Rosa, M. E.; Coutinho, J. A.; Mohamadou, A.; Freire, M. G. Glycine-Betaine Ionic Liquid Analogues as Novel Phase-Forming Components of Aqueous Biphasic Systems. *Biotechnol. Prog.* **2018**, *34*, 1205−1212.
(26) Hou, X.-D.; Liu, Q.-P.; Smith, T. J.; Li, N.; Zong, M.-H. Evaluation of Toxicity and Biodegradability of Cholinium Amino Acids Ionic Liquids. *PLoS One* **2013**, *8*, No. e59145.
(27) Zhao, G.; He, F.; Wu, C.; Li, P.; Li, N.; Deng, J.; Zhu, G.; Ren, W.; Peng, Y. Betaine in Inflammation: Mechanistic Aspects and Applications. *Front. Immunol.* **2018**, *9*, No. 1070.
(28) Gomes, J. M.; Silva, S. S.; Reis, R. L. Biocompatible Ionic Liquids: Fundamental Behaviours and Applications. *Chem. Soc. Rev.* **2019**, *48*, 4317−4335.
(29) Behnisch-Cornwell, S.; Laubenstein, G.; Bednarski, P. J. Studies of the Inhibitory Activities of Tiopronin and Mercaptosuccinic Acid on Glutathione Peroxidase and Their Cytotoxic and Antioxidant Properties. *Pharmazie* **2019**, *74*, 536−542.
(30) Rosa, E.; Diaferia, C.; Gallo, E.; Morelli, G.; Accardo, A. Stable Formulations of Peptide-Based Nanogels. *Molecules* **2020**, *25*, No. 3455.
(31) Klamt, A.; Jonas, V.; Bürger, T.; Lohrenz, J. C. W. Refinement and Parametrization of COSMO-RS. *J. Phys. Chem. A* **1998**, *102*, 5074−5085.
(32) *TURBOMOLE V7.2 2017, a Development of University of Karlsruhe and Forschungszentrum Karlsruhe GmbH, 1989-2007*; TURBOMOLE GmbH, 2010. Http://Www.Turbomole.Com.
(33) Steffen, C.; Thomas, K.; Huniar, U.; Hellweg, A.; Rubner, O.; Schroer, A. TmoleX—a Graphical User Interface for TURBOMOLE. *J. Comput. Chem.* **2010**, *31*, 2967−2970.
(34) *COSMOtherm, Release 19*; COSMOlogic GmbH & Co. KG, 2019.
(35) Kurnia, K. A.; Coutinho, J. A. P. Overview of the Excess Enthalpies of the Binary Mixtures Composed of Molecular Solvents and Ionic Liquids and Their Modeling Using COSMO-RS. *Ind. Eng. Chem. Res.* **2013**, *52*, 13862−13874.
(36) Lemaoui, T.; Hammoudi, N. E. H.; Alnashef, I. M.; Balsamo, M.; Erto, A.; Ernst, B.; Benguerba, Y. Quantitative Structure Properties Relationship for Deep Eutectic Solvents Using Sσ-Profile as Molecular Descriptors. *J. Mol. Liq.* **2020**, *309*, No. 113165.
(37) *Mathematica*, version 12.2; Wolfram Research Inc.: Champaign, IL, 2020.
(38) Bowers, K. J.; Chow, D. E.; Xu, H.; Dror, R. O.; Eastwood, M. P.; Gregersen, B. A.; Klepeis, J. L.; Kolossvary, I.; Moraes, M. A.; Sacerdoti, F. D.; Salmon, J. K.; Shan, Y.; Shaw, D. E. In *Scalable Algorithms for Molecular Dynamics Simulations on Commodity Clusters*, SC '06: Proceedings of the 2006 ACM/IEEE Conference on Supercomputing, 2006; p 43. https://doi.org/10.1109/SC.2006.54.
(39) *Schrödinger Release 2021-1: Desmond Molecular Dynamics System; Maestro-Desmond Interoperability Tools*; D. E. Shaw Research: New York, NY, 2021.
(40) Frisch, M. J.; Trucks, G. W.; Schlegel, H. B.; Scuseria, G. E.; Robb, M. A.; Cheeseman, J. R.; Scalmani, G.; Barone, V.; Petersson, G. A.; Nakatsuji, H.; Li, X.; Caricato, M.; Marenich, A. V.; Bloino, J.; Janesko, B. G.; Gomperts, R.; Mennucci, B.; Hratchian, H. P.; Ortiz, J. V.; Izmaylov, A. F.; Sonnenberg, J. L.; Williams-Young, D.; Ding, F.; Lipparini, F.; Egidi, F.; Goings, J.; Peng, B.; Petrone, A.; Henderson, T.; Ranasinghe, D.; Zakrzewski, V. G.; Gao, J.; Rega, N.; Zheng, G.; Liang, W.; Hada, M.; Ehara, M.; Toyota, K.; Fukuda, R.; Hasegawa, J.;

https://doi.org/10.1021/acsomega.1c03864
ACS Omega 2021, 6, 32460−32474

Ishida, M.; Nakajima, T.; Honda, Y.; Kitao, O.; Nakai, H.; Vreven, T.; Throssell, K.; Montgomery, J. A., Jr.; Peralta, J. E.; Ogliaro, F.; Bearpark, M. J.; Heyd, J. J.; Brothers, E. N.; Kudin, K. N.; Staroverov, V. N.; Keith, T. A.; Kobayashi, R.; Normand, J.; Raghavachari, K.; Rendell, A. P.; Burant, J. C.; Iyengar, S. S.; Tomasi, J.; Cossi, M.; Millam, J. M.; Klene, M.; Adamo, C.; Cammi, R.; Ochterski, J. W.; Martin, R. L.; Morokuma, K.; Farkas, O.; Foresman, J. B.; Fox, D. J.; et al. *Gaussian 16*, revision C.01; Gaussian, Inc.: Wallingford, CT, 2016.

(41) Méndez-Morales, T.; Carrete, J.; Bouzón-Capelo, S.; Pérez-Rodríguez, M.; Cabeza, O.; Gallego, L. J.; Varela, L. M. MD Simulations of the Formation of Stable Clusters in Mixtures of Alkaline Salts and Imidazolium-Based Ionic Liquids. *J. Phys. Chem. B* **2013**, *117*, 3207−3220.

(42) Rabideau, B.; Ismail, A. Mechanisms of Hydrogen Bond Formation between Ionic Liquids and Cellulose and the Influence of Water Content. *Phys. Chem. Chem. Phys.* **2015**, *17*, 5767−5775.

(43) Eckert, F. *COSMOtherm User's Manual*; COSMOlogic GmbH & Co, 2005.

(44) Bavoh, C. B.; Partoon, B.; Lal, B.; Gonfa, G.; Foo Khor, S.; Sharif, A. M. Inhibition Effect of Amino Acids on Carbon Dioxide Hydrate. *Chem. Eng. Sci.* **2017**, *171*, 331−339.

(45) Ghatee, M. H.; Zare, M.; Moosavi, F.; Zolghadr, A. R. Temperature-Dependent Density and Viscosity of the Ionic Liquids 1-Alkyl-3-Methylimidazolium Iodides: Experiment and Molecular Dynamics Simulation. *J. Chem. Eng. Data* **2010**, *55*, 3084−3088.

(46) Yuan, W.-L.; Yang, X.; He, L.; Xue, Y.; Qin, S.; Tao, G.-H. Viscosity, Conductivity, and Electrochemical Property of Dicyanamide Ionic Liquids. *Front. Chem.* **2018**, *6*, No. 59.

(47) Vadiraj, K. T.; Belagali, S. L. Spectrophotometric Determination of Copper (II) in Industrial Effluent Samples Using Sulfanilic Acid as a Ligand System. *Bulg. Chem. Commun.* **2014**, *162*, 447−451.

(48) Gonzalez-Miquel, M.; Massel, M.; DeSilva, A.; Palomar, J.; Rodriguez, F.; Brennecke, J. F. Excess Enthalpy of Monoethanolamine + Ionic Liquid Mixtures: How Good Are COSMO-RS Predictions? *J. Phys. Chem. B* **2014**, *118*, 11512−11522.

(49) Jumbri, K.; Kassim, M. A.; Yunus, N. M.; Abdul Rahman, M. B.; Ahmad, H.; Abdul Wahab, R. Fluorescence and Molecular Simulation Studies on the Interaction between Imidazolium-Based Ionic Liquids and Calf Thymus DNA. *Processes* **2020**, *8*, No. 13.

(50) Zhang, S.; Huo, F. Angstrom Science: Exploring Aggregates from a New Viewpoint. *Green Energy Environ.* **2016**, *1*, 75−78.

(51) Dong, K.; Zhang, S.; Wang, J. Understanding the Hydrogen Bonds in Ionic Liquids and Their Roles in Properties and Reactions. *Chem. Commun.* **2016**, *52*, 6744−6764.

(52) Novoselov, N. P.; Sashina, E. S.; Petrenko, V. E.; Zaborsky, M. Study of Dissolution of Cellulose in Ionic Liquids by Computer Modeling. *Fibre Chem.* **2007**, *39*, 153−158.

(53) Swatloski, R. P.; Spear, S. K.; Holbrey, J. D.; Rogers, R. D. Dissolution of Cellose with Ionic Liquids. *J. Am. Chem. Soc.* **2002**, *124*, 4974−4975.

(54) Wang, S.; Stubbs, J.; Siepmann, J.; Sandler, S. Effects of Conformational Distributions on Sigma Profiles in COSMO Theories. *J. Phys. Chem. A* **2005**, *109*, 11285−11294.

(55) Nakashima, T.; Kimizuka, N. Controlled Self-Assembly of Amphiphiles in Ionic Liquids and the Formation of Ionogels by Molecular Tuning of Cohesive Energies. *Polym. J.* **2012**, *44*, 665−671.

(56) Shamay, Y.; Shah, J.; Işık, M.; Mizrachi, A.; Leibold, J.; Tschaharganeh, D. F.; Roxbury, D.; Budhathoki-Uprety, J.; Nawaly, K.; Sugarman, J. L.; Baut, E.; Neiman, M. R.; Dacek, M.; Ganesh, K. S.; Johnson, D. C.; Sridharan, R.; Chu, K. L.; Rajasekhar, V. K.; Lowe, S. W.; Chodera, J. D.; Heller, D. A. Quantitative Self-Assembly Prediction Yields Targeted Nanomedicines. *Nat. Mater.* **2018**, *17*, 361−368.

https://doi.org/10.1021/acsomega.1c03864
ACS Omega 2021, 6, 32460−32474